Coherent Surface Plasmon Polariton Amplification via Free Electron Pumping

Ye Tian (tianye@siom.ac.cn)
Shanghai Institute of Optics and Fine Mechanics https://orcid.org/0000-0002-5618-5951
Dongdong Zhang
Shanghai Institute of Optics and Fine Mechanics, Chinese Academy of Sciences
https://orcid.org/0000-0001-8627-7016
Yushan Zeng
Shanghai Institute of Optics and Fine Mechanics https://orcid.org/0000-0001-5668-506X
Yafeng Bai
Shanghai Institute of Optics and Fine Mechanics
Zhongpeng Li
Shanghai Institute of Optics and Fine Mechanics
Ruxin Li
Shanghai Institute of Optics and Fine Mechanics

Physical Sciences - Article

Keywords:

Posted Date: April 21st, 2022

DOI: https://doi.org/10.21203/rs.3.rs-1572967/v1

Version of Record: A version of this preprint was published at Nature on November 2nd, 2022. See the published version at https://doi.org/10.1038/s41586-022-05239-2.

Title: Coherent Surface Plasmon Polariton Amplification via Free Electron Pumping

Authors: Dongdong Zhang[1,2]†, Yushan Zeng[1]†, Yafeng Bai[1]*, Zhongpeng Li[1], Ye Tian[1,2]*, Ruxin Li[1,2,3]*.

Affiliations:

[1]State Key Laboratory of High Field Laser Physics and CAS Center for Excellence in Ultra-intense Laser Science, Shanghai Institute of Optics and Fine Mechanics, Chinese Academy of Sciences; Shanghai 201800, P. R. China

[2]Center of Materials Science and Optoelectronics Engineering, University of Chinese Academy of Sciences; Beijing, 100049, P. R. China.

[3]School of Physical Science and Technology, ShanghaiTech University, Shanghai, P. R. China

*Corresponding author. Email: tianye@siom.ac.cn; baiyafeng@siom.ac.cn; ruxinli@mail.siom.ac.cn

†These authors contributed equally to this work.

Abstract: Surface plasmonic with its unique confinement of light is expected to be a cornerstone for future compact radiation sources and integrated photonics devices. The energy transfer between light and matter is a defining aspect that underlies recent studies on optical surface-wave-mediated spontaneous emissions. But coherent stimulated emission, being omnipresent in every laser system, remains to be realized and revealed in the optical near fields unambiguously and dynamically. Here, we present the coherent amplification of Terahertz surface plasmon polaritons via free electron stimulated emission. We demonstrate the evolutionary amplification process with a frequency redshift and lasts over 1-mm interaction length. The complementary theoretical analysis predicts a 100-order surface wave growth when a properly phase-matched electron bunch is used, which lays the ground for a stimulated surface wave light source and may facilitate capable means for matter manipulation, especially in the Terahertz band.

Exploiting the intensive confinement of light of the photonic quasiparticles[1] – which can be plasmonic or photonic – is now becoming a prerequisite for developing extremely compact radiation sources and breaking into the strong coupling regime. Surface plasmon polaritons (SPPs) [2-4] are a mixture of charge density wave and electromagnetic fields that can provide drastically altered photonic densities. Correspondingly, modulating the intensity, spectral, and spatiotemporal signatures of the SPPs can profoundly influence the light-matter properties during the interaction.

The motivation to accommodate the interplay between electrons and SPPs is longstanding and diverse, as light-matter interaction inside the SPPs can exhibit extraordinary properties that are otherwise inaccessible. At optical frequencies, infrared SPPs have been demonstrated to allow forbidden transitions in an atom system[5], building on-chip radiation sources[6-8], and even verifying the quantum nature of light[9]. Nonetheless, in both these cases, their realizations have relied on the precise control and detection of the probe electron beams (such as the photon-induced near-field electron microscopy, PINEM[10,11]); but the opposite situation – the tailoring and the spatiotemporal characterization of the SPPs field – even some decades after its initial recognition[12], is still nascent and awaits further explorations. Especially in the spectroscopic band beyond the optical frequencies, where the resonance frequency of many phonon polaritons modes resides[13-15], versatile promising prospects include effective excitation of polariton modes in two-dimensional materials[14,15], forming terahertz detectors[16] and molecular sensors[17] can be envisioned in the far-infrared and Terahertz (THz) frequency range.

In this regard, it is intriguing to extend the SPPs frequency from infrared to the Terahertz band to see what new capabilities could be enabled. In the elementary light emission processes like spontaneous radiation, conventional light-matter interactions within the SPPs disregard the phase variance between different electrons because of particular challenges pertaining to phase matching[6,18]. Despite the acquirement of attosecond electron pulses is already feasible[19-22], such difficulty still presents a major obstacle towards the experimental realization and characterization of coherent stimulated emission of free electrons within the SPPs field. But the THz SPPs can considerably alleviate this strenuous demand: the propagating and stretched wavelength nature of the THz SPPs provides much more tolerability of the coherence of the free electron beam[23,24]. In practice, this translates into an attainable femtosecond electron bunch for exploring the prospects of coherent stimulated emission inside the THz SPPs.

Here, employing electrons as an emitter rather than probing tools, we propose a concept for coherent Terahertz SPPs light source via free electrons stimulated emission directly into the THz SPPs. We demonstrate experimentally the spatiotemporally resolved generation, amplification, and dephasing processes of the THz SPPs both in terms of the magnetic and electric near field evolution, presenting unambiguously the SPPs amplification dynamics with a coherent interaction length over 1 mm. Our experiment achieves this coherent SPPs amplification through the inelastic scattering of the laser-produced electrons. Under our current experimental situations, a radiation frequency redshift from 0.65 THz to 0.34 THz is observed and theoretically analyzed. The results hence represent the first experimental demonstration of stimulated emission by free electrons in the light-matter interaction with photonic quasiparticles. In addition, we also prove theoretically that the radiation power can be further magnified by 100 orders with a phase-matched condition, laying the grounds for a foreseeable free-electron laser (FEL) SPPs laser.

Theoretically, the amplification process of the SPPs is an integral part of the elementary electron-SPPs interactions, whose opposite situation – namely, the electron absorbs photon energy – corresponds exactly to the increasingly promising area of dielectric laser accelerators (DLA) [25,26]. We compared our results with other typical electron-SPPs interactions, including DLA and PINEM, and bridge the different types of interplay in terms of the electron qualities relative to the SPPs. The connection we built conforms to a unified interaction process, whether characterized by quantum or classical electron energy losses (as in the PINEM and DLA), or by the discrete or continuous photon changes (as in HHG and our experiment), reconcile to the same physical picture which is only divided by phase-matching conditions and the coherence length of the electron beam.

Coherent SPPs amplification

In our scheme, coherent SPPs amplification is made possible by traversing an ultrashort free-electron pulse over a photonic structure that supports SPPs (Fig.1), such as a flat conductor surface or the recently burgeoning van der Waals materials like graphene[6,8,27]. Under a more general physical picture illustrated in the Feynman diagrams of (Fig.1b), the SPPs amplification process involves two-electron absorption/emission stages during interaction: (I) seed generation and (II) SPPs amplification via the electron-SPPs energy exchanges. While SPPs can be excited in the first stage either directly by irradiating a strong femtosecond laser pulse[28,29] or via free-space coupling with mode and momentum matched electromagnetic waves[30]. The initially excited SPPs are weak in terms of field strength for strong coupling effects. We henceforth refer to this structure-mode-matched polariton as the seed for the ensuing emission processes. When considering an electron pulse that is spatiotemporally shorter than the SPPs seed and co-propagates with the seed field, stimulated radiation commences as the copropagating electrons are decelerated by the SPP field. This process underlies the coherent SPPs amplification in stage two, where the emitted photons reinforce the SPPs on the optical medium.

We fulfill both processes by focusing a femtosecond laser pulse onto the photonic structure. The specific SPPs supporter used in our experiment is a thin bare metal wire that has been well-studied as "waveguides" for both THz SPPs and electrons[31-33]. With this specialized experimental setting (Fig.1a), the THz SPPs seed is formulated via the broadband spontaneous emission of the laser-accelerated electrons from within the wire and are mode matched to the waveguide structure.

The ensuing energy exchange between the electron and THz SPPs can transform into a PINEM-type interaction with adequate electron pulse coherence, that is, sufficiently long pulse duration and distinguishable energy divergence, as demonstrated in the discussion. But here, the laser-induced electron pulse, though being divergent in energy distribution and is far from monochromatic, can inherit the temporal duration and the focal spot size of the driving laser pulse at the beginning, and co-propagates with the THz SPPs over the wire surface. As shown below, the THz SPPs have larger dimensions than that of the initial electron pulse, permitting the second stage to take place before dephasing. Hence, the coherent stimulated emission demonstrated here can lead to strong SPPs fields in a way arduous by other means.

For example, the phase-matching requirement is substantially alleviated due to the larger spatial size of the THz SPPs, approving approximately 1100 μm coherent interaction length (or 4 ps duration) achieved with our experimental conditions. The femtosecond laser-induced electrons and the THz SPPs seed also allow for precise synchrony as well as substantial electron charge (about nano Coulomb) that is otherwise impossible.

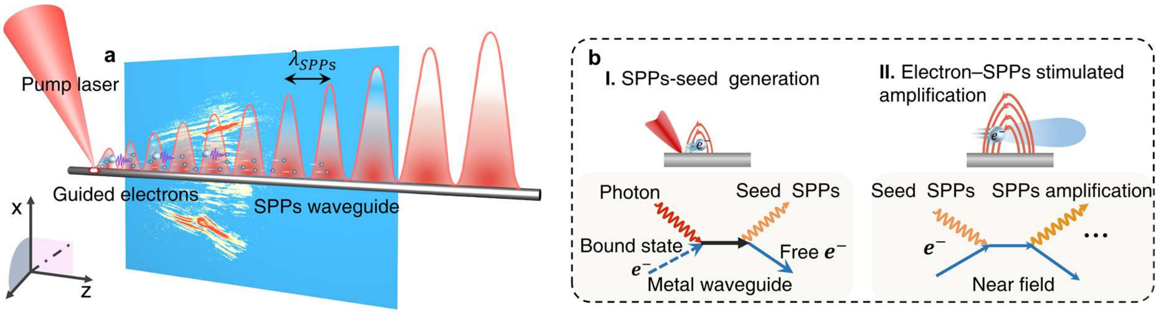

Fig. 1. Coherent SPPs amplification by stimulated emission. a. schematic illustrating the SPPs generation and amplification processes, in which the femtosecond laser-produced electron bunch coherently interacts with the weak seed field it spontaneously emitted in the first stage, resulting in the SPPs amplification. The color-coded map at the rear of the SPPs waveguide represents a near-field snapshot of the SPPs. **b.** Diagrammatic depiction of the seed generation (stage I) and the stimulated amplification (stage II) processes: a first-order spontaneous emission process followed by a high-order process where the ultrashort bunch duration can cause stimulated emission inside the instantaneous SPPs field.

Spatiotemporally resolved SPPs measurements

The experiments are performed on a bare metal wire with a diameter of 50 μm and a length of ~80mm. To dynamically record the electron interaction with the SPPs, we utilize an optical pump-probe method that is supplied by a Ti:sapphire femtosecond laser, as detailed in the supplementary material. Typically for resolving the interaction between electron and near field, this second pulse is generally frequency up-converted to allow photoemission of electron packets as the ultimate probing tool for the interaction process, like the PINEM. Recent advances in PINEM have provided spatiotemporal dynamics of a polariton propagation on a 2D material[34]. However, PINEM becomes less efficient in the mid-infrared and THz bands, because it relies on the minuscule discrimination of the electron energies that are separated by the photon energy and is restricted by the penetration depth of the electrons.

Our experiment demonstrates coherent THz SPPs amplification through the optical near field imaging, in which the time-resolved electromagnetic field evolution of the THz SPPs is captured separately via the magneto-optical Faraday effect and the electro-optical effect. For magnetic field characterization (see supplementary material), a 1 mm-thick, (111)-cut terbium gallium garnet ($Tb_3Ga_5O_{12}$, TGG) single crystal is placed parallel to the wire axis respectively at 500 μm, 750 μm, or 1000 μm distance. The magnetic field evolution of the SPPs dynamics can hence be probed via the polarization variations imprinted on the probe beam via a sequential snapshot. Alternatively, the electric field of the SPPs can be characterized similarly via a copropagating, temporally stretched (from 30 fs to 8.66 ps) probe beam that traverses through a zinc telluride (ZnTe) placed 3 cm downstream of the main beam focus (Fig.S1). Whereas the former provides the spatiotemporally resolved SPPs evolution, the latter enables characterization of the final state of the SPPs after the "walk-off".

We first investigate the SPPs field profiles using the Faraday geometry, recording the SPPs seed generation, propagation, amplification, and part of the dephasing stage (Fig.2a and movie S1) by scanning the relative time delay between the pump and probe beams. In the color-coded map displayed in Fig.2a, our experimental photo records of the SPPs identify two major lobes located equidistantly on both sides of the wire. After laser irradiance (defined as $\tau_d = 0$), the cross-section shapes of the SPPs exhibit a perceivable expansion both in volume and strength on the 500 μm near-field TGG. We deduce the maximum perceived magnetic field strength from the rotated polarization angle of the probe beam to be 5.11 Tesla at approximate

$\tau_d = 4.27\ ps$. Afterwards, the stamped SPPs field strength starts to saturate at this detection distance. A qualitative analysis of the SPPs wave packet profile on the TGG shows the SPPs intensity evolution as a function of the propagation distance, as demonstrated in Fig.2b. This growth unambiguously evidences the amplification process of the laser-induced SPPs on the wire.

Noteworthy, the field evolution recorded at different TGG distances to the wire axis has incommensurate time evolutions in Fig.2b. Such variances arise as a natural result of the SPPs generation and expansion processes, which can be accurately portraited only when all different detection distances are considered in a combined manner. We elaborate on this in the supplementary material, with the integrated magnetic energy evolution presented in Fig.2c. As a result, the absolute magnetic energy evolution detected by the TGG can be clarified as follows: the SPPs seed keeps growing during $\tau_d < 4.27\ ps$. But its instantaneous emitted polaritons are diminishing due to the electron pulse broadening and velocity mismatching with the SPPs, giving rise to the saturation stage ($4.27\ ps < \tau_d$) before they walk off.

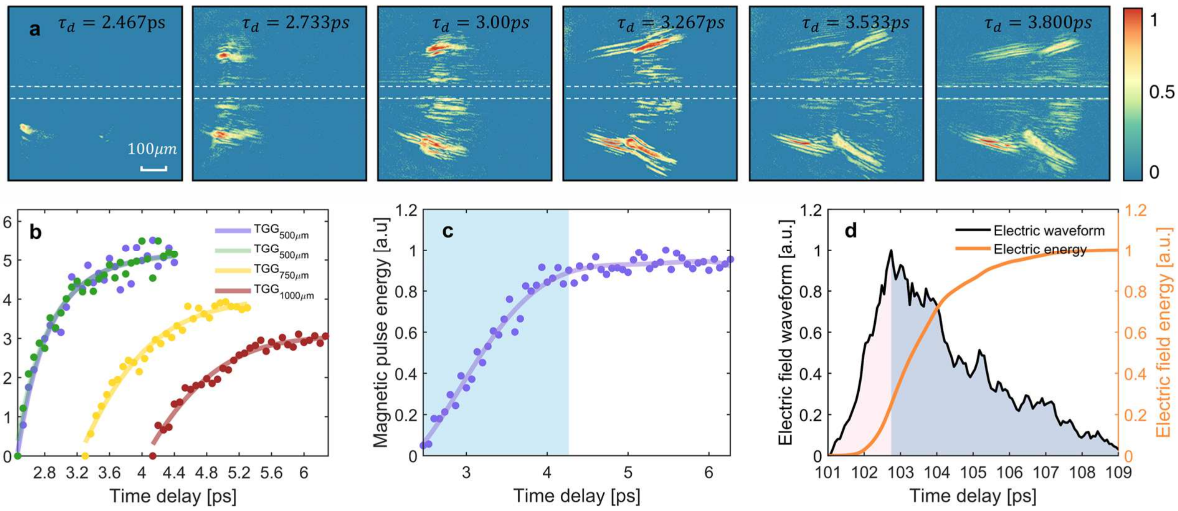

Fig. 2. Spatiotemporal dynamics of the electromagnetic field of the THz SPPs. a, p-polarized near-field snapshots of the THz SPPs magnetic field at different time delays on the 500 μm TGG crystal. The profiles show two discernible lobes located equidistantly on the two sides of the THz SPPs waveguide structure (i.e., the metal wire, as marked by the gray dashed line). τ_d=0 is defined as the laser irradiation moment. **b,** Measured time-depend magnetic field strength (dotted curves) of the THz SPPs on different TGG detection distances. We compare three magnetic field evolutions on the 500, 750, and 1000 μm TGG crystal, whose maximum magnetic fields of B= 5.11, 3.88, and 3.01 T are respectively reached at τ_d= 4.27, 5.30, and 6.27 ps. **c,** The partial magnetic field energy evolutions in space as integrated from different TGG sampling distances. It should be noted that, the spatial energy contained within the <500 μm vicinity to the wire surface is not included. The shaded background represents times at which the magnetic field energy is still rising. Afterwards, the electron and the SPPs are about to "walk-off". **d,** Derived THz SPPs waveform (black curve) from the single-shot electro-optical sampling. The data shows that the exponential amplification lasts for 1.73 ps (pink shaded area), after when though the emitted polaritons (gray shaded area) are declining due to the degraded electron coherence, the total SPPs energy (orange solid line) is still rising.

Figure 2d presents an example of the measured electric field waveform of the SPPs from the single-shot electro-optical sampling[35]. Intuitively, the obtained electric field waveform represents a final state of the SPPs after the entire interaction process, incorporating fingerprints that are derived independently from the coherent amplification, dephasing, and the propagation effects after walking off. Evidence of such features can be found in the rising/trailing edges of the electric field waveform. For example, as shown in Fig.2c, the ascending part (pink shaded area) of the electric field relates to the exponential amplification process, whose total electric field energy (orange line) shows a corresponding rise that lasts

1.73 ps. Afterwards, the growth rate slows down due to the degraded coherence of the electron beam and saturates at 4.43 ps, similar to that of the magnetic field measurement. Such equivalence originates from the microscopic origin of the SPPs generation, whose intensity proportionally depends on the electron-emitted photon quantity. In a similar vein, the dephasing duration can also be inferred from the trailing part of the waveform (Fig.2c, gray shaded area) to be about 6.32 ps, during when the generated SPPs though being declining, the accumulated SPPs energy (orange line) is still rising until they walk off about 8.05 ps after the laser irradiation.

Analysis of SPPs amplification

To illustrate the SPPs dynamics on the 500 μm near-field detection plane, we quantify the spatially acquired THz SPPs profiles as a function of time and propagation distance in Fig.3a. Intriguingly in this color-coded map, our experimental result identifies two divergent branches of the acquired spatial profiles: the first one with a weaker strength stays almost standstill during our picoseconds scanning time; and a stronger second branch undergoes intensity modifications and has a superluminal phase speed of $0.46 \pm 0.01\ mm/ps$ (or 1.53±0.04 c, where c is the vacuum speed of light) on the 500 μm crystal TGG. Here, we attribute this stagnant branch (branch II) to possible localized ionization effects by the electrons that may reduce the probe transmittance[36]. But the superluminal signals (branch I), comprising of a series of the field stamps when the wavefront traverses through the TGG, must have come from the propagating THz SPPs on the wire owing to its propagating nature bound to the wire waveguide[31]. We henceforth refer to this second signal (branch I) as the THz SPPs in the following text.

For qualitative analysis of the THz SPPs amplification process, we exclude the contribution from the first branch by intercepting the signal with only the branch I, and then fit the summed spatial profile with a Gaussian line shape at each time delay. Figure 3b presents a sequential series of the fitted THz SPPs spatial profiles, whose peaks outlined accurately the time-dependent intensity evolution of THz SPPs: at points where the THz SPPs reach their maximum, the wave packet has already propagated about 1.27 mm away from the laser focus, corresponding to a 4.28 ps time duration at 0.99c propagating speed[31].

The extraction of the THz SPPs signal also facilitates a more precise analysis of the spectral information concealed in the electron-SPPs interaction. Since the laser-excited SPPs are in nature a half-cycle wave polariton without reversed field component, the spectral map of the THz SPPs is reconstructed with an emitting geometry hypothesizing that the THz SPPs are emitted into free space immediately at each delay time. We discuss the validity of this spectral processing in the supplementary material. From the resultant spectral map in Fig.3c there is a notable frequency bandwidth narrowing and center frequency downshift, from 0.65 THz to 0.34 THz, as the delay time evolves from 2.53 to 4.40 ps. This finding reveals a glimpse of the underlying physical process of the THz SPPs amplification: as the electron is decelerated in the copropagating SPPs field, it slips towards the rear part of the semi-cycle SPPs field where a long trailing edge of the radiation waveform is produced, as exemplified by the gray shaded area presented in Fig.2d. As a result, this temporal broadening of the SPPs waveform would lead to the broadened spatial file and a frequency redshift in the subsequent SPPs spectra.

The spectral modifications can also find theoretical explanations in the general Lienard-Wiechert potential of coherent radiation emission. Explicitly, the power of an electron bunch with electron number N and velocity v, as a function of frequency (ω) and solid angle (Ω), can be expressed by:

$$\frac{d^2I}{d\omega d\Omega} = N^2 f(\omega) \times \frac{e^2\omega^2}{4\pi^2 c} \left| \int_{-\infty}^{\infty} \vec{n} \times (\vec{\beta} \times \vec{n}) e^{i\omega[t - \vec{n}\cdot\vec{r}(t)/c]} dt \right|^2$$

where $\vec{\beta} = \vec{v}/c$ is the normalized velocity, $\vec{n}$ is the unit vector of observation direction, and $\vec{r}(t)$ is the location of the electron bunch center. The form factor $f(\omega)$ denotes the Fourier transform of electrons' spatial distribution within the bunch. For a coherent bunch with pulse duration σ, this form factor can be described by a simple analytical expression of $f(\omega) = \exp[(-\omega\sigma/c)^2]^{37}$, which quantitatively illustrates how smaller frequency can occupy lager share of the spectral weight in the radiation spectrum.

In the simplified picture ignoring the helical movement of the electrons, the radiated SPPs are generated in a copropagating manner with the electrons. This occurrence of SPPs frequency downshift and narrowing is also corroborated in a finite difference time domain (FDTD) simulation following a 30 fs duration Gaussian beam departed from a 50 μm diameter wire, as exemplified in (Fig.3d-f). Comparing the experimentally observed frequency down-conversion with the analytical results in Fig.3f the spectral map of the simulated results implies a good agreement in both the spectral bandwidth and spectral center with the experimental results.

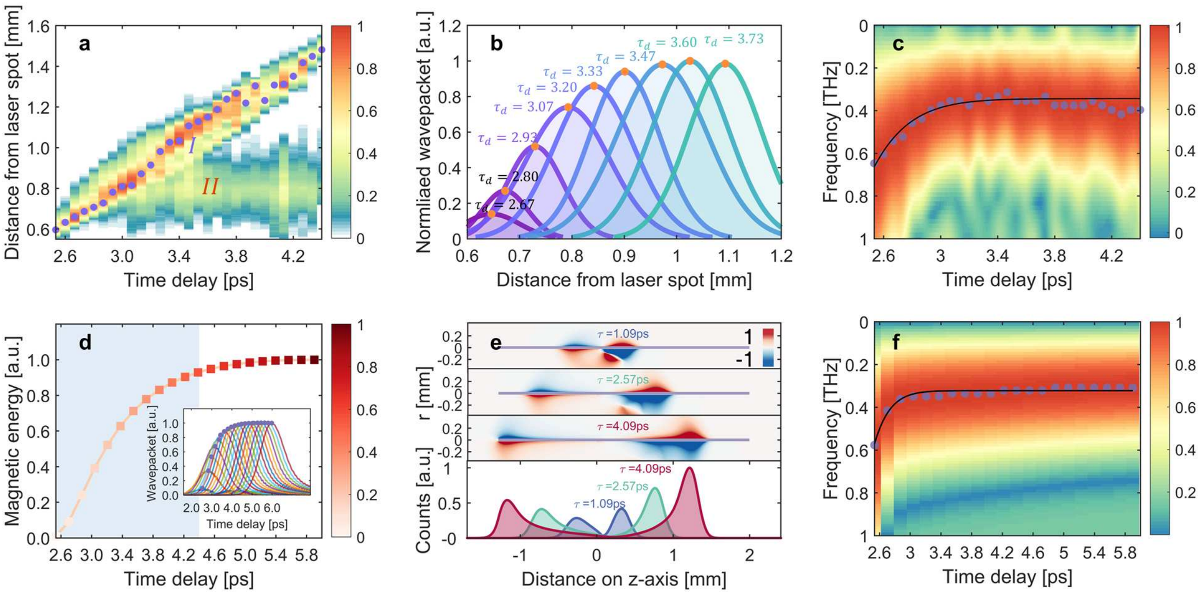

Fig. 3. Spatial and spectral properties of the THz SPPs during the amplification process. a, THz SPPs profiles as a function of time and propagation distance mapped on the 500 μm near-field TGG plane. There are two branches of signal, in which only branch I is unlocalized, corresponding to the propagating THz SPPs. The purple dots mark the Gaussian fit peaks of the THz SPPs wave packet as outlined in **b. c,** The spectral map of the immediate THz SPPs as a function of time and propagation distance that are acquired on the 500 μm TGG plane. **(d to f)** Simulated THz SPPs amplification dynamics, showing a correspondent magnetic field energy and waveform evolution **d,** instantaneous field profiles on the wire **e,** and the spectral map **f,** during the interaction process. The signal shows an obvious signal growth with frequency down-conversion from 0.54 to 0.32 THz, similar to the experimental results.

Towards a stimulated SPPs light source

Our present experimental result realizes coherent electron emission in the context of photonic quasiparticles with laser-produced electron bunches. Representing a particular example of free electron and light field interactions, the massively energy-divergent electrons contained in the femtosecond pulse can reasonably be regarded as a spatiotemporally limited point in the long THz field - as opposed to a plane-wave that is described in the quantum languages. As a result, a classical treatment is found to yield good agreement with our experimental observations. This conformity, together with the stimulated SPPs amplification, relates to the recent experiment and simulation studies drawing on spontaneous emission/absorption processes but exhibiting a quantum electron-light energy transfer. Yet, an open and essential question still lingers in the physical processes described above: in what circumstances should quantum effects be manifested, as demonstrated in PINEM-type experiments; and how can we maximize the stimulated radiation power for practical applications?

To shed light on the underlying energy exchange between the free electron and light field, we firstly examined the energy modulations of a quasi-monochromatic electron beam after traversing a copropagating photonic quasiparticle, like the SPPs field described in this work. By implementing an ultrashort electron pulse that is much shorter than the spatial width of the SPPs wavelength λ, the electron loses or gains energy inside the SPPs field, analogous to the situation inside a dielectric laser accelerator (DLA). And the energy exchanges in the form of photon emission/absorption when the electron is decelerated/accelerated in an electric field with a field strength of E. Hence, the radiation energy modulation ΔE can be simplified as $\Delta E = eEz = eEv\Delta t$, where v denotes the electron velocity, z denotes the electron interaction distance inside the SPPs, and Δt represents the lasting time of the interaction.

From the uncertainty principle $\Delta E \Delta t > \hbar/2$, one may expect classical or quantum effects to be dominant since the single-photon emission can only depend on probability (i.e. quantum) when this inequality is unsatisfied, resembling the situation of atomic transitions inside a bound-electron system. Hence, a rough estimation yields at most a 2.5 femtometer interaction length for the quantum effect to be pronounced for a $10^8\ V/m$ electric field. On the contrary, in the classical approximation of micrometer and larger scales, radiation is generated in an uninterrupted manner whose frequency is inseparably reliant on the interaction time $\Delta t > \lambda$ for a deceleration process, giving rise to lower frequency components in the radiation spectrum.

We then deduce separately the radiation scaling and electron energy losses with the point-like electron source inside the SPPs field. As demonstrated in supplementary material, the electrons can exchange energy with the SPPs field effectively once their phase is precisely controlled, resembling the process of Rabi oscillation in a two-level system. The simulation in Fig.4b (blue solid line) considers a complete phase matching condition for the maximum radiation power. When supposing a monochromatic electron bunch train, each with ~0.16nC charge (and ~0.5 nC in total), ~100 fs pulse duration, and 0.6c moving speed[28] that interacts with a 0.3 THz multicycle SPPs, the simulation shows the free-electron laser (FEL) type growth due to the constructive interference of coherent radiation between different electrons. In comparison with the experimental one with a rapidly dephasing electron beam, the optimized electron pulse intensifies the radiated THz SPPs power by 100 orders, leading to a prospective stimulated SPPs radiation source that may find applications in devices that require super-intense strong surface field, such as exciting phonon polaritons modes[14,15], flipping the spin of atoms[38] and so on.

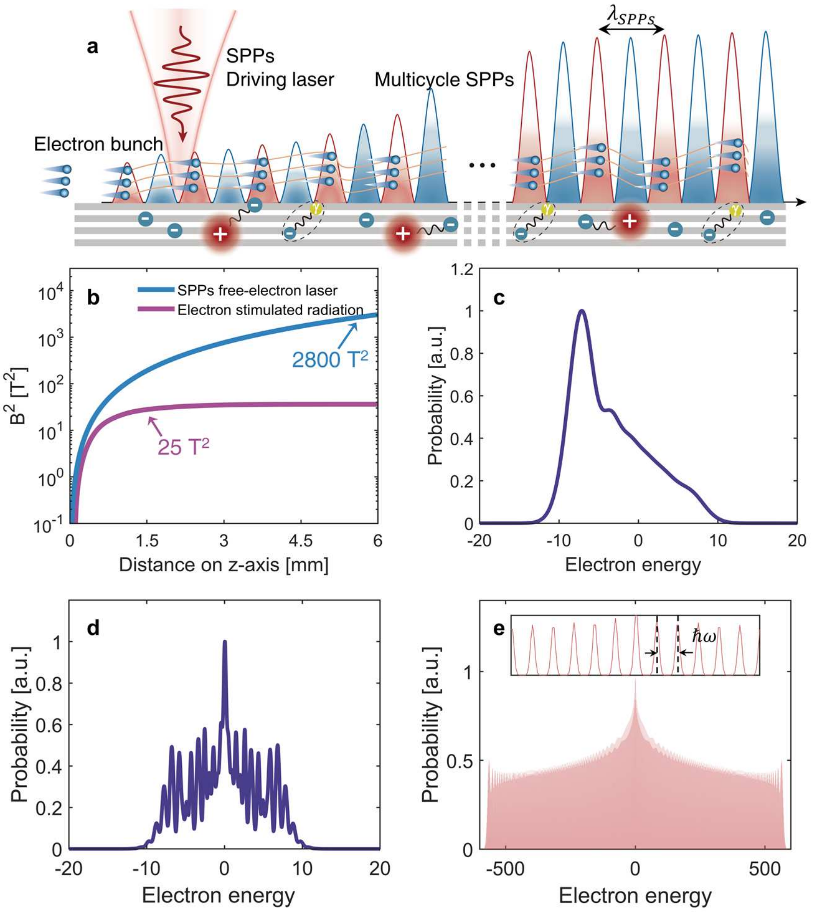

Fig. 4. Influence of electron coherence length on the quantum effects and SPPs amplification. a, Schematic showing a sub-wavelength electron pulse train interacting with a multicycle SPPs field on a photonic structure. Under such a scenario, coherent stimulated emission is allowed to give rise to the free-electron laser (FEL) type SPPs amplification as exemplified by the blue curve in **b**, In comparison with the growth rate acquired from our experiment results (magenta solid line), the super-radiation situation can further magnify our experimental outcome by 100 orders using phase-matched monochromatic electrons, paving the path towards a stimulated SPPs light source. The magnetic energy density is acquired 500-µm from the waveguide surface. (**c**-**e**), Semi-classical simulations result of the electron energy loss spectrum with different electron coherence lengths and phase matching conditions. For the case of an electron pulse that is much shorter than the SPPs cycle (1/10 of the SPPs period), continuous electron energy modulation is observed as illustrated by the moment t=0 **c**, In comparison, discrete energy changes are obtained for a long electron pulse (10 times the SPPs period), with larger gain/loss appearing for phase-matched conditions. The detailed semiclassical theory for the calculation is elaborated in the supplementary material.

For the electron energy loss in such conditions, the eventual electron energy spectrum is calculated as a function of injection time (delay) into the SPPs field. Here, we present one snapshot at delay t=0 in Fig.4c, where a continuous electron energy modulation is obtained. In such a scenario, the SPPs field imparts its energy to the electron via an immediate momentum kick, giving rise to the continuing energy modulation that straightforwardly samples the THz field waveforms (i.e., streaking).

In contrast with a point-like particle, a continuous electron beam epitomizes the quantum situation as it is inherent a plane-wave quantum wave function. Using a long electron beam (10 times the field period), our calculation produces the electron energy modulations exemplifying the typical sidebands separated by the photon quanta (Fig.4d and e). Here, Fig.4d represents a phase mismatched situation, where the electron bunch speed is incommensurate with the phase velocity of the SPPs field, and eventually leads to the deteriorated interacting length and hence the reduced photon quanta of about 20.

Figure 4e presents the electron energy loss spectrum for a phase-matched condition by hypothesizing the electron speed to be equal to that of the SPPs. This condition allows for a 60-fold surge of exchanged photon numbers than the mismatched situation described in Fig.4d. To facilitate such extensive energy exchange, various efforts including using dielectric geometries[18], microresonators[39], and photonic integrated circuits[40] have been devised to achieve precise phase matching. However, this is still a formidable task with the stringently spatially confined light field and the substantially slowed photonic quasiparticles. But with the longer wavelength of the THz SPPs, we envisage much stronger control over fundamental light-matter interactions at handy providing suitable electron pulse and detection means.

Summary and outlook

In conclusion, we have demonstrated the coherent THz SPPs amplification via stimulated emission by free electrons, observing the spatiotemporal evolution of the THz SPPs and a 2-fold frequency redshift from 0.65 THz to 0.34 THz during the emission process. The stimulated emission follows from the femtosecond electron pulse duration and the much larger THz SPPs size which allows constructive interference to take place. As a result, a coherent interaction length over 1 mm is obtained, which is much greater than that in the infrared band with more sophisticated phase matching methods.

Thinking beyond the laser-generated divergent electron beam in our experiment, a specifical purpose-customed electron beam is expected to relate different types of interactions, electron energy loss (radiation) or gain (acceleration), classical or quantum. This is because qualitatively different electron characteristics, for example, regarding the roles of electron coherence length and phase matching velocity, give rise to distinctive photon and electron energy loss spectrums including radiation amplification, streaking, and PINEM-type experiments. In the amplification situation, for instance, the precisely phase-matched electron beam could lead to super-intense SPPs that are otherwise impossible to achieve. Such prospect will enable various applications of this concept in the light-matter manipulation and plasmon-based devices where a super-intense surface wave is required.

References:

1 Rivera, N. & Kaminer, I. Light–matter interactions with photonic quasiparticles. *Nature Reviews Physics* **2**, 538-561, doi:10.1038/s42254-020-0224-2 (2020).

2 Barnes, W. L., Dereux, A. & Ebbesen, T. W. Surface plasmon subwavelength optics. *Nature* **424**, 824-830, doi:10.1038/nature01937 (2003).

3 Berini, P. & De Leon, I. Surface plasmon-polariton amplifiers and lasers. *Nature Photonics* **6**, 16-24, doi:10.1038/nphoton.2011.285 (2012).

4 Torma, P. & Barnes, W. L. Strong coupling between surface plasmon polaritons and emitters: a review. *Reports on Progress in Physics* **78**, 013901, doi:10.1088/0034-4885/78/1/013901 (2015).

5 Rivera, N., Kaminer, I., Zhen, B., Joannopoulos, J. D. & Soljacic, M. Shrinking light to allow forbidden transitions on the atomic scale. *Science* **353**, 263-269, doi:10.1126/science.aaf6308 (2016).

6 Wong, L. J., Kaminer, I., Ilic, O., Joannopoulos, J. D. & Soljačić, M. Towards graphene plasmon-based free-electron infrared to X-ray sources. *Nature Photonics* **10**, 46-52, doi:10.1038/nphoton.2015.223 (2015).

7 Hu, H. *et al.* Surface Dyakonov–Cherenkov radiation. *eLight* **2**, 2, doi:10.1186/s43593-021-00009-5 (2022).

8 Pizzi, A. *et al.* Graphene Metamaterials for Intense, Tunable, and Compact Extreme Ultraviolet and X-Ray Sources. *Adv Sci (Weinh)* **7**, 1901609, doi:10.1002/advs.201901609 (2020).

9 Dahan, R. *et al.* Imprinting the quantum statistics of photons on free electrons. *Science* **373**, eabj7128, doi:10.1126/science.abj7128 (2021).

10 Barwick, B., Flannigan, D. J. & Zewail, A. H. Photon-induced near-field electron microscopy. *Nature* **462**, 902-906, doi:10.1038/nature08662 (2009).

11 Park, S. T., Lin, M. & Zewail, A. H. Photon-induced near-field electron microscopy (PINEM): theoretical and experimental. *New Journal of Physics* **12**, 123028, doi:10.1088/1367-2630/12/12/123028 (2010).

12 Ritchie, R. H. Plasma Losses by Fast Electrons in Thin Films. *Physical Review* **106**, 874-881, doi:10.1103/PhysRev.106.874 (1957).

13 Kojima, S., Kitahara, H., Nishizawa, S. & Takeda, M. W. in *11th International Conference on Phonon Scattering in Condensed Matter (PHONONS 2004).* 2674-2677 (2004).

14 Giles, A. J. *et al.* Ultralow-loss polaritons in isotopically pure boron nitride. *Nature Materials* **17**, 134-139, doi:10.1038/nmat5047 (2018).

15 Ma, W. *et al.* In-plane anisotropic and ultra-low-loss polaritons in a natural van der Waals crystal. *Nature* **562**, 557-562, doi:10.1038/s41586-018-0618-9 (2018).

16 Cai, X. *et al.* Plasmon-Enhanced Terahertz Photodetection in Graphene. *Nano Letters* **15**, 4295-4302, doi:10.1021/acs.nanolett.5b00137 (2015).

17 Rodrigo, D. *et al.* Mid-infrared plasmonic biosensing with graphene. *Science* **349**, 165-168, doi:10.1126/science.aab2051 (2015).

18 Dahan, R. *et al.* Resonant phase-matching between a light wave and a free-electron wavefunction. *Nature Physics* **16**, 1123-1131, doi:10.1038/s41567-020-01042-w (2020).

19 Feist, A. *et al.* Quantum coherent optical phase modulation in an ultrafast transmission electron microscope. *Nature* **521**, 200-203, doi:10.1038/nature14463 (2015).

20 Morimoto, Y. & Baum, P. Diffraction and microscopy with attosecond electron pulse trains. *Nature Physics* **14**, 252-256, doi:10.1038/s41567-017-0007-6 (2017).

21 Kozak, M., Schonenberger, N. & Hommelhoff, P. Ponderomotive Generation and Detection of Attosecond Free-Electron Pulse Trains. *Phys Rev Lett* **120**, 103203, doi:10.1103/PhysRevLett.120.103203 (2018).

22 Zhou, C. *et al.* Direct mapping of attosecond electron dynamics. *Nat. Photonics* **15**, 216-221, doi:10.1038/s41566-020-00730-6 (2021).

23 Caldwell, J. D. *et al.* Low-loss, infrared and terahertz nanophotonics using surface phonon polaritons. *Nanophotonics* **4**, 44-68, doi:10.1515/nanoph-2014-0003 (2015).

24 Zhang, X. *et al.* Terahertz surface plasmonic waves: a review. *Advanced Photonics* **2**, 014001 doi:10.1117/1.Ap.2.1.014001 (2020).

25 England, R. J. *et al.* Dielectric laser accelerators. *Reviews of Modern Physics* **86**, 1337-1389, doi:10.1103/RevModPhys.86.1337 (2014).

26 Adiv, Y. *et al.* Quantum Nature of Dielectric Laser Accelerators. *Physical Review X* **11**, 041042, doi:10.1103/PhysRevX.11.041042 (2021).

27 Avetissian, H. K., Avchyan, B. R., Matevosyan, H. H. & Mkrtchian, G. F. Free-electron nanolaser based on graphene plasmons. *Laser Physics* **31**, 055801, doi:10.1088/1555-6611/abeb20 (2021).
28 Tian, Y. *et al.* Femtosecond-laser-driven wire-guided helical undulator for intense terahertz radiation. *Nature Photonics* **11**, 242-246, doi:10.1038/nphoton.2017.16 (2017).
29 Zeng, Y. *et al.* Guiding and emission of milijoule single-cycle THz pulse from laser-driven wire-like targets. *Opt Express* **28**, 15258-15267, doi:10.1364/OE.390764 (2020).
30 Zheng, Z., Kanda, N., Konishi, K. & Kuwata-Gonokami, M. Efficient coupling of propagating broadband terahertz radial beams to metal wires. *Opt. Express* **21**, 10642-10650, doi:10.1364/oe.21.010642 (2013).
31 Wang, K. L. & Mittleman, D. M. Metal wires for terahertz wave guiding. *Nature* **432**, 376-379, doi:10.1038/nature03040 (2004).
32 Wang, K. & Mittleman, D. M. Dispersion of surface plasmon polaritons on metal wires in the terahertz frequency range. *Phys Rev Lett* **96**, 157401, doi:10.1103/PhysRevLett.96.157401 (2006).
33 Nakajima, H., Tokita, S., Inoue, S., Hashida, M. & Sakabe, S. Divergence-free transport of laser-produced fast electrons along a meter-long wire target. *Phys Rev Lett* **110**, 155001, doi:10.1103/PhysRevLett.110.155001 (2013).
34 Kurman, Y. *et al.* Spatiotemporal imaging of 2D polariton wave packet dynamics using free electrons. *Science* **372**, 1181-1186, doi:10.1126/science.abg9015 (2021).
35 Jiang, Z. P. & Zhang, X. C. Electro-optic measurement of THz field pulses with a chirped optical beam. *Applied Physics Letters* **72**, 1945-1947, doi:10.1063/1.121231 (1998).
36 Sarkisov, G. S. *et al.* Fountain effect of laser-driven relativistic electrons inside a solid dielectric. *Applied Physics Letters* **99**, 131501, doi:10.1063/1.3641862 (2011).
37 Carr, G. L. *et al.* High-power terahertz radiation from relativistic electrons. *Nature* **420**, 153-156, doi:DOI 10.1038/nature01175 (2002).
38 Schlauderer, S. *et al.* Temporal and spectral fingerprints of ultrafast all-coherent spin switching. *Nature* **569**, 383-387, doi:10.1038/s41586-019-1174-7 (2019).
39 Kfir, O. *et al.* Controlling free electrons with optical whispering-gallery modes. *Nature* **582**, 46-49, doi:10.1038/s41586-020-2320-y (2020).
40 Henke, J. W. *et al.* Integrated photonics enables continuous-beam electron phase modulation. *Nature* **600**, 653-658, doi:10.1038/s41586-021-04197-5 (2021).

Acknowledgments: This research was supported by the National Natural Science Foundation of China (grants No. 11922412, 11874372, 12104473, 12104471). Shanghai Pilot Program for Basic Research – Chinese Academy of Science. Shanghai Branch Key Research Program of Frontier Sciences, CAS. Youth Innovation Promotion Association of Chinese Academy of Sciences. Shanghai Sailing Program (grant No. 20YF1454900, 21YF1453900). We thank J. Zi, and L. Shi from Fudan University for the fruitful discussions regarding the SPPs properties.

Author contributions: Y. T. and R. L conceived and supervised the project. D. Z., Z. L., Y. B. conducted the experimental measurements. Y. B. and Y. T. developed the theory. D. Z., Y. B. and Y. Z. performed the data analyses. Y. Z., D. Z., and Y. B. wrote the manuscript. All authors reviewed and discussed the manuscript and made substantial contribution to it.

Competing interests: Authors declare that they have no competing interests.

Data availability: The data supporting the findings of this study are available from the corresponding author upon reasonable request.

Supplementary Files

This is a list of supplementary files associated with this preprint. Click to download.

- TGG0825500SM.mp4
- SupplementaryMaterials.pdf